A Fully Noble Metal-Free Photosystem Based on Cobalt- Polyoxometalates Immobilized in a Porphyrinic Metal- Organic-Framework for Water Oxidation

Grégoire Paille, Maria Gomez-Mingot, Catherine Roch-Marchal, Benedikt Lassalle-Kaiser, Pierre Mialane, Marc Fontecave, Caroline Mellot-Draznieks, Anne Dolbecq

▶ **To cite this version:**

Grégoire Paille, Maria Gomez-Mingot, Catherine Roch-Marchal, Benedikt Lassalle-Kaiser, Pierre Mialane, et al.. A Fully Noble Metal-Free Photosystem Based on Cobalt- Polyoxometalates Immobilized in a Porphyrinic Metal- Organic-Framework for Water Oxidation. Journal of the American Chemical Society, 2018, 10.1021/jacs.7b11788 . hal-02081087

HAL Id: hal-02081087
https://hal.science/hal-02081087v1

Submitted on 27 Mar 2019

HAL is a multi-disciplinary open access archive for the deposit and dissemination of scientific research documents, whether they are published or not. The documents may come from teaching and research institutions in France or abroad, or from public or private research centers.

L'archive ouverte pluridisciplinaire **HAL**, est destinée au dépôt et à la diffusion de documents scientifiques de niveau recherche, publiés ou non, émanant des établissements d'enseignement et de recherche français ou étrangers, des laboratoires publics ou privés.

A Fully Noble Metal-Free Photosystem Based on Cobalt-Polyoxometalates Immobilized in a Porphyrinic Metal-Organic-Framework for Water Oxidation

Grégoire Paille,[§,‡] Maria Gomez-Mingot,[‡] Catherine Roch-Marchal,[§] Benedikt Lassalle-Kaiser,[†] Pierre Mialane,[§] Marc Fontecave,[*,‡] Caroline Mellot-Draznieks,[*,‡] and Anne Dolbecq[*,§]

§Institut Lavoisier de Versailles, UMR CNRS 8180, Université de Versailles Saint-Quentin en Yvelines, Université Paris-Saclay, 45 Avenue des Etats-Unis, 78035 Versailles Cedex, France
‡Laboratoire de Chimie des Processus Biologiques, UMR CNRS 8229, Collège de France, Université Pierre et Marie Curie, PSL Research University, 11 Place Marcelin Berthelot, 75231 Paris Cedex 05, France
†Synchrotron Soleil, l'Orme des Merisiers, Saint-Aubin, 91192 Gif-sur-Yvette Cedex, France

ABSTRACT: The sandwich-type polyoxometalate (POM) $[(PW_9O_{34})_2Co_4(H_2O)_2]^{10-}$ was immobilized in the hexagonal channels of the Zr(IV) porphyrinic MOF-545 hybrid framework. The resulting composite was fully characterized by a panel of physicochemical techniques. Calculations allowed identifying the localization of the POM in the vicinity of the Zr_6 clusters and porphyrin linkers constituting the MOF. The material exhibits a high photocatalytic activity and good stability for visible-light-driven water oxidation. It thus represents a rare example of an all-in-one fully noble metal-free supramolecular heterogeneous photocatalytic system, with the catalyst and the photosensitizer within the same porous solid material.

INTRODUCTION

In the current energetic transition, one major challenge concerns the development of noble metal-free, selective, efficient, and recyclable heterogeneous photocatalysts. In this respect, the design of new multifunctional porous and robust hybrid solids bringing together i) catalysis, ii) light capture and iii) porosity is a particularly attractive alternative to create novel "three-in-one" photoactive catalysts. Due to their porosity and the functional tunability of their organic linkers,[1] metal-organic frameworks (MOFs) represent an ideal platform. MOFs may incorporate redox catalytic centers while organic linkers may behave as light-harvesting units capable of transferring electrons to neighboring catalytic centers.[2] Furthermore, synthetic or post-synthetic strategies allow grafting or encapsulating additional functional units within the MOF's pores.[3] For example some of us have recently reported the heterogenization of a Rh-based molecular catalyst as the constitutive linker of a mixed-linker UiO-67, providing an active and recyclable solid catalyst for CO_2 photoreduction.[4] Polyoxometalates (POMs) can also play the role of functional catalytic units. POMs are soluble anionic metal oxide clusters of d-block transition metals in high oxidation states (usually W^{VI}, $Mo^{V,VI}$, $V^{IV,V}$) exhibiting properties that can be exploited in many fields.[5] In particular, POMs can undergo multielectron redox transformations conferring them catalytic redox activity,[6] while being also known as proton and electron relays.[7] Several studies have reported the successful incorporation of POMs into MOFs cavities leading to the so-called POM@MOFs.[8] In that context, one of the most studied MOFs for encapsulation is the highly porous MIL-101,[9] but HKUST-1,[10] and more recently ZIF[11] and Zr-based MOFs[12] have also been investigated as robust host structures. Besides, photocatalytic properties of POMs in the presence of molecular porphyrins were investigated in homogeneous conditions for various reactions such as reduction of silver cations,[13] hydrogen[14] and oxygen[15] evolution reactions. These studies evidenced that porphyrins may be efficiently used for visible light sensitization of POMs.

In the present work, we report the design of the first noble metal-free heterogeneous photosystem using a POM as a catalyst immobilized in the pores of a porphyrinic MOF. We selected MOF-545,[16] also known as PCN-222[17] and MMPF-6,[18] for its unique properties: i) a high surface area thanks to hexagonal channels large enough to accommodate POMs (Figure 1), ii) an excellent chemical and thermal stability, iii) the ability to capture visible light due to the porphyrin linker. It has also proved being an efficient host for biomimetic iron complexes.[19] We selected the $[(PW_9O_{34})_2Co_4(H_2O)_2]^{10-}$ POM (named $P_2W_{18}Co_4$, Figure 1) as the catalytically active guest. This POM exhibits a tetracobalt oxide core sandwiched between two $[PW_9O_{34}]^{9-}$ polyoxotungstate cages and is known for its homogenous photocatalytic activity for oxygen evolution reaction (OER) in the presence of a ruthenium-based molecular photosensitizer.[20] The new POM@MOF photosystem reported here was fully characterized and evaluated for its photocatalytic performances for water oxidation. Besides, density functional theory calculations provided insights into the unique structural features of the POM-MOF interface.

RESULTS AND DISCUSSION

Synthesis. The encapsulation of the POMs was performed by mild aqueous impregnation of MOF-545 with an excess of the alkaline salt of the $P_2W_{18}Co_4$ POM, monitored by UV-Vis spectroscopy of the supernatant solution. Once the MOF was added to the solution for impregnation, the intensity of the Co-based d-d absorption at 566 nm gradually decreased and stabilized after 6 hours (Figure S1a). The amount of POMs deduced from the difference in absorbance of the solution before and after impregnation is ~ 1 POM per unit of MOF and represents the amount of POMs encapsulated in the MOF pores plus the amount of POMs adsorbed at the surface of the MOF particles.

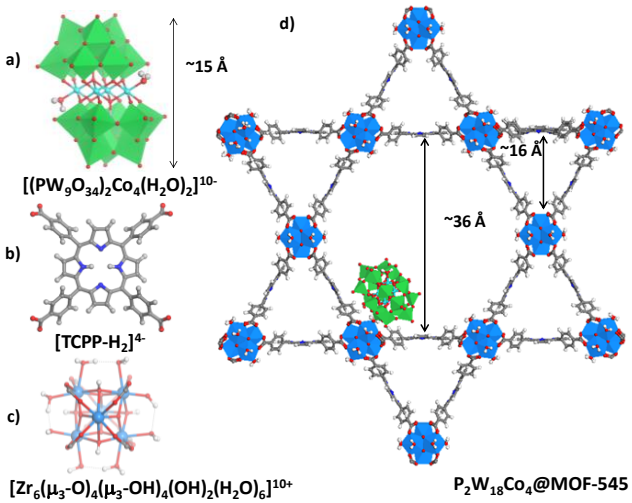

Figure 1. POM@MOF-545 components. (a) $P_2W_{18}Co_4$ POM; (b) TCPP-H_2 linker; (c) Zr-based unit; (d) $P_2W_{18}Co_4$@MOF-545. The position of the POM is obtained from computations (see text). WO_6, green polyhedra; ZrO_8, blue polyhedral or spheres; Co, cyan spheres; O, red spheres; C, H, grey; N, dark blue.

The POM@MOF is then filtrated and washed with water. The absorbance of the first washing solution indicates that ~0.45 POM per unit of MOF is released during washing (Figure S1c). The following washing solutions no longer contain POMs. These experiments show that the amount of encapsulated POMs is estimated ~0.55 POM per unit of MOF i.e. 0.18 POM per $\{Zr_6\}$ units. The composite material, named $P_2W_{18}Co_4$@MOF-545, was then synthesized in large quantities, carefully washed with water and analyzed by various techniques.

Characterizations. Elemental analysis (Table S1) allows proposing the formula $[Zr_6O_{16}H_{18}][TCPP\text{-}H_2]_2[P_2W_{18}Co_4]_{0.2}\bullet 26H_2O$ and confirms the amount of encapsulated POM determined by UV-Vis spectroscopy. SEM-EDS elemental mapping shows a uniform distribution of the Zr, Co and W elements in the bulk material of impregnated MOF (Figure S2) and indicate average Zr/Co and Zr/W ratios consistent with the results of elemental analysis (Table S2). STEM-HAADF images coupled to EDS mapping of the various elements were also recorded (Figure 2). On the one hand, they show that the solid material consists of rod-like shape crystals of 2.4 x 0.4 x 0.4 μm average dimensions and nicely confirm the localization of the POM-specific W and Co elements within the MOF crystals, while the MOF host is characterized by Zr, N and O mapping. On the other hand, they also show that the POM species exhibit higher concentrations at both extremities of the crystal rods, consistent with the alignment of the channels of the MOF along the *c* axis, i.e. the longest dimension of the rods**.** Thermogravimetric analysis (TGA) measurements show mass losses of ca. 53% for the $P_2W_{18}Co_4$@MOF-545 composite and 65% for the bare MOF-545 (Figure S3). These weight losses are assigned to water removal, linker decomposition and formation of inorganic oxides. The lower weight loss of $P_2W_{18}Co_4$@MOF-545 with respect to the bare MOF-545 is in agreement with the presence of POMs in the POM@MOF material (Table S3). While this adventitious population is observed during encapsulation by UV-vis spectroscopy, it is absent in samples characterized by elemental analysis, carried out after the washing steps. In the proposed formula, the negative charge of the POMs is likely compensated by the protonation of the hybrid framework as confirmed by the absence of alkaline cations shown by EDS analysis (Table S2). Consistently, the isoelectric point of MOF-545 is at pH 8,[21] indicating that the MOF is indeed cationic under the pH synthetic conditions. Relying on IR spectroscopy[22] and DFT[23] studies on the related NU-1000 material, we thus propose the following proton localization on the charged Zr_6-clusters, $[Zr_6(\mu_3\text{-}O)_4(\mu_3\text{-}OH)_4(OH)_2(H_2O)_6]^{10+}$.

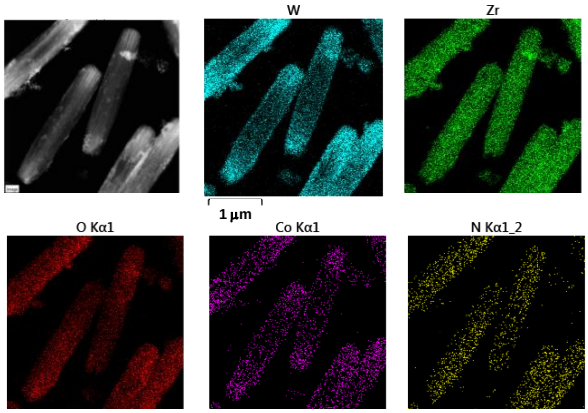

Figure 2. STEM-HAADF images of POM@MOF-545 and EDS mapping of the various elements contained in the POM (W, Co, O) and MOF (Zr, O, N).

Brunauer–Emmett–Teller (BET) surface area measurements (Figure 3a) calculated from the N_2 adsorption/desorption isotherms show the expected correlation between decreased surface areas and POM encapsulation, from 2080 $m^2\ g^{-1}$ for the bare MOF to 1180 m^2g^{-1} for $P_2W_{18}Co_4$@MOF-545. Furthermore, the pore distribution is also found to be strongly modified upon POMs' encapsulation (Figure S4). These measurements indicate that the POMs are indeed located in the MOF's largest pores, i.e. the hexagonal channels. Indeed a decrease in intensity of the peak attributed to the hexagonal pores is observed while the peak attributed to the triangular pores remains unchanged. This is not surprising considering their large diameter (~36 Å) compatible with the adsorption of the bulky POMs species (~16 Å) unlike the triangular channels which have too small diameters (~16 Å) (Figure 1).

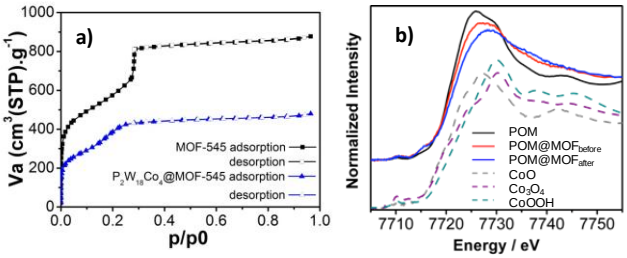

Figure 3. (a) BET N_2 adsorption/desorption isotherms (77 K, P/P_0 = 1 atm.) of MOF-545 and $P_2W_8Co_4$@MOF-545. (b) XANES spectra of $P_2W_{18}Co_4$, $P_2W_{18}Co_4$@MOF-545 before and after catalysis, compared to related oxides.

The powder X-ray diffraction patterns of the bare MOF-545 and of the POM@MOF-545 composite (Figure S5) confirm that the crystallinity of the MOF host is maintained upon incorporation of the POM. The UV-Vis spectrum of $P_2W_{18}Co_4$@MOF-545 merges the characteristic bands of the MOF-545 at 390 and 400-700 nm, and those of the $P_2W_{18}Co_4$ POMs around 300 and 560 nm (Figure S6). Co K-edge X-ray absorption near edge spectra (XANES) of $P_2W_{18}Co_4$ and $P_2W_{18}Co_4$@MOF-545 were also

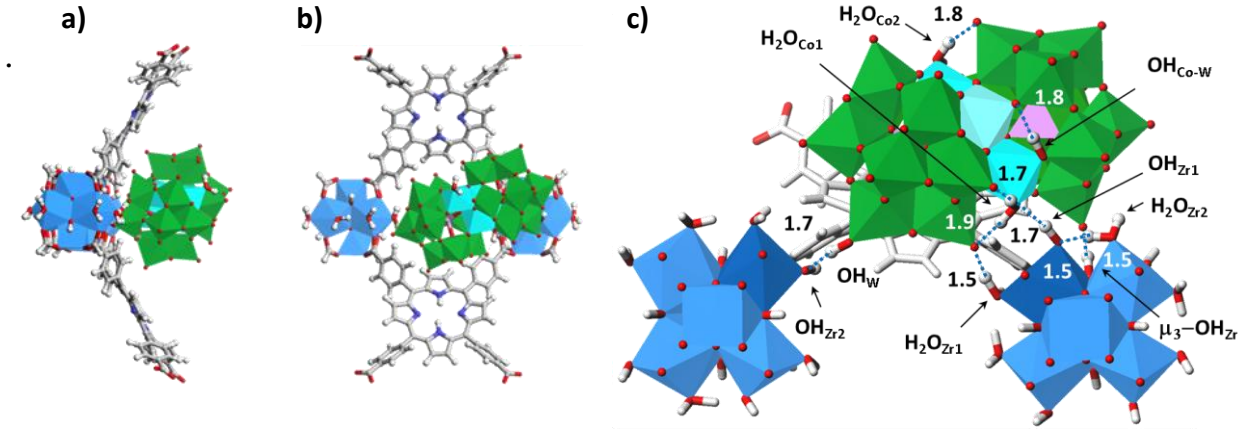

Figure 4. Computed position of the $P_2W_{18}Co_4$ POM in MOF-545. (a) "Side" and (b) "top" views of the POM positioned between two Zr_6-clusters and two porphyrins. (c) Detailed lateral view of the POM-MOF interface and the hydrogen-bond network. One porphyrin is not represented for more clarity. Distances are given in Å. The external Co centers with water molecules ligands are highlighted in bright cyan

collected (Figure 3b). The similarity of the two spectra shows that the POM is intact after its immobilization within the MOF. The slight difference can be attributed to the electrostatic interaction between the POMs and the MOF, as observed for $P_2W_{18}Co_4$@MIL-101(Cr).[9c] Also, the comparison with reference cobalt oxides indicates the absence of degradation into the typical cobalt oxides known to be active for OER activity (Co_3O_4 or CoOOH).

DFT Calculations. To probe the {POM, MOF} potential energy surface and the most likely positions of the POM within the pores, we applied a combination of simulated annealing (SA) calculations and DFT-D3 level geometry optimizations (see text and Figures S7-S10 in SI for details). SA calculations show that the insertion of POMs occurs exclusively in the hexagonal channels of MOF-545 in line with the above findings (Figure S8). Figures 4a and 4b illustrate the position of the POM in MOF-545's channels as obtained from DFT-D3 level geometry optimization of the lowest energy position extracted from SA calculations, in a "side" view and a "top" view, respectively. This computed position reflects the chemical environment that the POM may adopt when adsorbed at the MOF's internal surface before catalysis. The POM is located in the vicinity of two Zr_6-clusters connected through two porphyrinic linkers. It is stabilized by a particularly dense network of hydrogen bonds that involve –OH groups and H_2O molecules belonging either to the POM or the MOF. As illustrated in Figure 4c, these H-bonds are concentrated at the POM-MOF interface mainly around one of two external Co-OH_2 centers of the tetracobalt oxide core. One Zr_6-cluster allows the anchoring of the POM to the MOF's surface through strong H-bonds: i) between the terminal water of the Co1 center, H_2O_{Co1}, and an $–OH_{Zr1}$ group of the MOF, ($O(H_2O_{Co1})\cdots H(OH_{Zr1})$=1.7 Å); ii) between oxygen atoms of the WO_6 moieties and hydrogen atoms of the MOF, the H atoms belonging to a μ_3-OH group ($O_W\cdots H(\mu_3\text{-}OH_{Zr})$=1.5 Å) and a terminal water molecule of the Zr-cluster ($O_W\cdots H(H_2O_{Zr1})$=1.5 Å). The other Zr_6-cluster provides further stabilization of the POM thanks to a more peripheral H-bond (with respect to the Co-core) between terminal hydroxyl groups at the POM-MOF interface ($HO_W\cdots OH_{Zr2}$=1.7 Å). DFT calculations indicate that the host-guest interactions (mainly hydrogen bonds and electrostatic interactions) are very strong (~ 176 kcal mol^{-1}). Interestingly, the computed structure reveals a shuttling of protons at the POM-MOF interface from the MOF to the POM (see SI for details). The basic character of the POM is thus apparent with the formation of the two terminal –OH groups at its surface, labeled OH_{Co-W} and OH_W (see Figure 4c). They both result from the transfer of H atoms from terminal water molecules coordinated to the Zr atoms (Zr1 and Zr2, respectively, in dark blue in Figure 4c) to oxygen atoms of the WO_6 moieties, leaving OH_{Zr1} and OH_{Zr2} hydroxyls at the MOF's surface. The protonation of the bridging oxygen Co-O-W found here is in line with previous computational studies,[24] showing that Co-O-W bridges are the most basic ones. Overall, DFT calculations reveal that the POM-MOF interface strongly affects the local arrangement of H_2O molecules and –OH groups towards optimized H-bond type host-guest interactions, when compared to the isolated POM and MOF counterparts.

The recent theoretical study by Hill and Poblet[24] establishes Co-OH_2 units as the reactive site. Interestingly, our DFT results suggest that the Co-OH_2 catalytic site exposed at the MOF-POM interface is hosted within a hydrophilic (water and -OH rich) catalytic pocket which may provide ideal shuttling of protons and water molecules transiting from the solvent.

Photocatalytic activities. The photocatalytic OER activity of $P_2W_{18}Co_4$@MOF-545 was studied under visible light irradiation in pH 8 borate buffer and with $Na_2S_2O_8$ as the electron acceptor. As shown in Figure 5, O_2 was formed immediately upon exposure to light and increased linearly with time (TOF = 40 10^{-3} s^{-1} calculated for the first 15 min) before reaching a plateau after 1 h of reaction. Addition of a fresh solution of the sacrificial acceptor, $Na_2S_2O_8$, resulted in a new cycle of O_2 production with the same initial TOF (Figure S11). These results clearly prove that the system is mainly limited by the consumption of the electron acceptor. The effect of pH was studied, showing that the optimal pH value is ~8 (Figure S12). The results show indeed that the photocatalytic OER activity of the POM@MOF is lower at pH 7.5 and 8.5 than at pH 8. This may be due to the chemical instability of the POM at pH > 8 and the too acidic conditions for doing the OER when pH < 8.[25a] $P_2W_{18}Co_4$@MOF-545 showed a good activity during OER with a turnover number (per POM) of 70 after 1 hour reaction. Control experiments with i) no catalyst, ii) no irradiation, iii) MOF-545 with no encapsulated POM, or iv) a

solution containing the TCCP-H_2 linker and $P_2W_{18}Co_4$, did not show any significant O_2 evolution (Figure 5 and Figure S13).

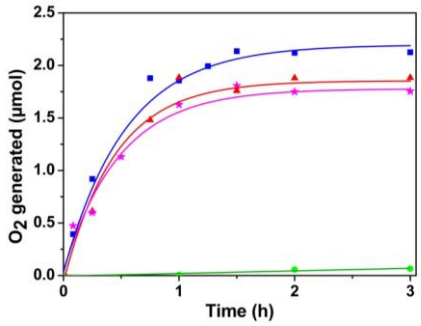

Figure 5. Kinetics of visible-light-driven O_2 production measured by GC analysis over 0.5 mg of $P_2W_{18}Co_4$@MOF-545 (blue square), $P_2W_{18}Co_4$@MOF-545 recycled once (red triangle), twice (pink stars), 131 µM TCPP-H_2 and 13 µM $P_2W_{18}Co_4$ in solution (green circle).[25] Reaction conditions: 5 mM $Na_2S_2O_8$ in 2 mL of 80 mM borate buffer solution, pH 8, visible light (λ > 420 nm, 280 W).

The fact that TCCP-H_2 is unable to photosensitize $P_2W_{18}Co_4$ seems to contradict its ability to do it in the context of the POM@MOF. This difference may be understood in light of the recent results from Xu *et al.*[26] who reported that the incorporation of the TCPP-H_2 linker into the MOF-545 results in its valence band (HOMO) shifting from 1.24 to 1.35 V *vs.* NHE, thus increasing the driving force for water oxidation. The reaction mechanism should thus imply the following steps: (i) light capture by the porphyrin; (ii) one-electron oxidation of the excited state by the sacrificial electron acceptor; (iii) one-electron oxidation of the POM; (iv) after accumulation of 4 oxidizing equivalents on the POM, oxidation of water into O_2 (Figure 6).

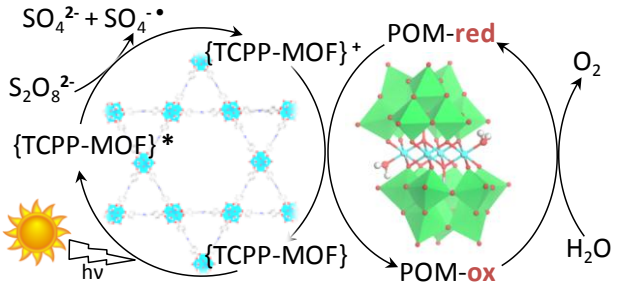

Figure 6. Schematic representation of the proposed mechanism for the light-driven OER by $P_2W_{18}Co_4$@MOF-545.

In order to assess the recyclability of the photocatalytic material, the reaction was performed using the POM@MOF recovered after 3 h, and assayed in an additional photocatalytic run. A decrease of the TON of ~11 % was then observed (Figure 5). A third recovery-catalytic cycle was performed, showing an even smaller loss of TON (<5 %). Even though the final TONs are lower, we note that the initial rates remain similar. Moreover, TGA (Figure S3), XRD (Figure S5) and EDS analyses (Table S2) did not show any difference between the composite before and after the reaction, confirming its stability upon photocatalysis. The XANES spectrum (Figure 3b) recorded on $P_2W_{18}Co_4$@MOF-545 after a 3 h photocatalytic experiment shows a slight shift of the main edge position towards higher energies (0.4 eV) with respect to the initial material. Given that the pre-edge region did not present any change in intensity or any new peak, we exclude a net change in the cobalt oxidation state. We rather attribute this shift to changes in the local environment of the cobalt and exclude any drastic modification in its structure. These results are in line with the studies of Schiwon *et al.* [27] who demonstrated the stability of the same POM under chemically induced OER.

CONCLUSIONS

In summary, this is the first time that a porphyrinic POM@MOF system, devoid of any noble metal, is used for visible-light water oxidation in aqueous solution. While very few studies have achieved the stable incorporation of the two key components (the photosensitizer and the catalysts) of a photosystem within a solid MOF, for CO_2 or proton photoreduction,[19,26,31] this is also the first such system developed for water photooxidation. Calculations provided valuable information on the localization of the POMs in the pores, especially a detailed view of the POM-MOF interface that reveals strong host-guest interactions. Such a computational approach has never been reported so far for POM@MOF materials. The above results show that the unique activity of this POM@MOF photosystem benefits from two main factors: i) immobilization of the porphyrin as a ligand in the MOF increases its oxidizing power and ii) the confinement of POMs inside the pores of the MOF plays a key role in the stabilization of the cobalt POM's catalytic site while the POM-MOF interface provides key components (-OH, labile water molecules) relevant to the OER mechanism. Furthermore this new POM@MOF photosystem takes full advantage of the already known stabilization of the porphyrin excited state in this kind of hybrid framework.[26] The POM@MOF composite is stable and easily reusable. Among others, work is in progress in order to study the influence of the metalation of the porphyrin on the catalytic activity.[32] The screening of various POMs as guest species is also under study. Overall, this work opens the way to a whole family of porphyrin-based MOFs as light-sensitive hosts for the elaboration of noble metal-free heterogeneous and recyclable photosystems.

EXPERIMENTAL SECTION

$Na_{10}[(PW_9O_{34})_2Co_4(H_2O)_2]$ ($Na_{10}P_2W_{18}Co_4$)[28] and tetrakis(4-carboxyphenyl)porphyrin TCPP-H_2[29] were synthesized according to reported procedures. All of the other reagents were purchased from commercial sources and used as received.

Synthesis of MOF-545. MOF-545 was synthesized according to a slightly modified procedure.[30] $ZrOCl_2$•$8H_2O$ (325 mg, 1.0 mmol) and TCPP-H_2 (65 mg, 0.086 mmol) were dissolved in 80 mL of DMF and 2.5 mL of dichloroacetic acid in a 100 mL round-bottomed flask. All reactants were stirred briefly before heating. The mixture was heated to 130 °C for 15 h, and allowed to cool down to room temperature. The solid was recovered by centrifugation, washed with DMF, and acetone. The resulting powder was dispersed in 25 mL of DMF and 2.5 mL of 1 M HCl and refluxed for 2 h. After centrifugation, the solid was washed with DMF and acetone and then soaked into acetone overnight. The powder was washed with acetone and diethyl ether and dried overnight in a 90°C oven. 85 mg of a purple powder were collected (yield 83 % based on TCPP-H_2). EDS analysis have shown the presence of chlorine with a Zr/Cl ratio equal to ~4 therefore the formula of the MOF was assumed to be $[Zr_6O_{16}H_{17.5}][C_{48}H_{26}N_4O_8]_2Cl_{1.5}$•$14H_2O$. Anal. Calc. (found) (2700 g mol^{-1}): C 42.71 (42.05), H 3.64 (2.76), N 4.15 (3.99).

Synthesis of $P_2W_{18}Co_4$@MOF-545. 100 mg of MOF-545 (3.7×10^{-5} mol) was dispersed in 20 mL of a 5 mM solution of $Na_{10}P_2W_{18}Co_4$. The suspension was stirred for 6 h. POM@MOF-

545 was collected by centrifugation and washed with water, acetone and diethyl ether and finally dried overnight in a 90°C oven. Finally, 150 mg (yield 86% based on MOF-545) of a dark purple powder was collected.

Protocol for UV-vis studies. Several vials were prepared with 10 mg of MOF-545 suspended in 2 mL of a 5 mM solution of $Na_{10}P_2W_{18}Co_4$. The suspensions were stirred for various times ranging from 30 min to 24 h. The solutions were centrifuged before recording their UV-vis spectrum.

Physical methods. Infrared (IR) spectra were recorded on a Nicolet 30 ATR 6700 FT spectrometer. Powder X-ray diffraction (PXRD) data were obtained on a Bruker D5000 diffractometer using Cu radiation (1.54059 Å). Energy dispersive spectroscopy (EDS) measurements were performed on a JEOL JSM 5800LV apparatus. STEM-HAADF pictures were recorded on a JEM 2100 PLUS. N_2 adsorption isotherms were obtained at 77 K using a BELsorp Mini (Bel, Japan). Prior to the analysis, approximately 30 mg of sample were evacuated at 90°C under primary vacuum overnight. Thermogravimetry analyses (TGA) were performed on a Mettler Toledo TGA/DSC 1, STARe System apparatus under oxygen flow (50 mL min^{-1}) at a heating rate of 5°C min^{-1} up to 800°C. Elemental analyses were performed by CREALINS, 5 Rue de la Doua, 69100 Villeurbanne, France (heavy elements, ICP-AES analyses) and by the Service de Microanalyse of CNRS, ICSN, 91198 Gif-sur-Yvette, France (C, H, N). UV-vis spectra were recorded on a Perkin Elmer Lambda 750 UV/Vis/NIR spectrometer using a quartz cuvette with a 1 cm long optical pathway. X-ray absorption spectra were recorded on the LUCIA beamline of SOLEIL at a ring energy of 2.75 GeV and a current of 500 mA. The incident energy was selected using a Si(111) double-crystal monochromator and calibrated to the first inflection point of a titanium foil (E = 4966.4 eV). Measurements were performed in fluorescence mode using a Bruker fluorescence detector.

Photocatalytic activity measurements. Solutions containing 2.5 mg of $P_2W_{18}Co_4$@MOF-545 and 5 mM $Na_2S_2O_8$ were prepared in 80 mM $B(OH)_3$ pH = 8 buffer (adjusted using NaOH 1M), and give a total volume of 10 mL. These samples were prepared in anaerobic and dark conditions and were sonicated for 5 min. Then, 2 mL of this mixture were transferred to a 1 cm quartz cuvette, sealed with a septum, degassed in nitrogen for 15 min and finally placed into a temperature controlled block at 20°C. After 5 hour the material was collected from the solution through centrifugation, washed with water and put in suspension into a fresh 2 mL 5 mM $Na_2S_2O_8$ in 80 mM $B(OH)_3$ pH = 8 in order to show its recyclability. A similar procedure was used for solutions containing 5 mM $Na_2S_2O_8$, 1 mM $Ru(bpy)_3Cl_2$ and 2 µM $P_2W_{18}Co_4$ in the same borate buffer. The cuvettes were irradiated with a 280 W Xenon Light Source equipped with a 325 nm cut-off filter (Asahi Spectra). During irradiation, the samples were vigorously stirred and 50 µL aliquots of the headspace were analyzed by gas chromatography analysis (Shimadzu GC-2014) with a thermal conductivity detector and a Quadrex column. O_2 measurements were quantified according to the corresponding calibration curves.

ASSOCIATED CONTENT

The Supporting Information is available free of charge on the ACS Publications website at DOI:xx.
Experimental and computational details (PDF).

AUTHOR INFORMATION

Corresponding Authors

* anne.dolbecq@uvsq.fr
* caroline.mellot-draznieks@college-de-france.fr
* marc.fontecave@college-de-france.fr

ACKNOWLEDGMENTS

This work was supported by the Ministère de l'Enseignement supérieur, de la Recherche et de l'Innovation, CNRS and UVSQ. We acknowledge financial support from the Fondation de l'Orangerie. The calculations have been performed using the HPC resources from GENCI (CINES) through Grant 2016-097343. AD and GP thank Youven Benseghir for his participation to the synthesis and UV-Vis studies. Sandra Casale is gratefully acknowledged for recording the TEM images.

REFERENCES

(1) (a) Furukawa, H.; Cordova, K. E.; O'Keeffe, M.; Yaghi, O. M. *Science* **2013**, *341*, 123044. (b) Wang, C.; Liu, X.; Demir, N. K.; Chen, J. P.; Li, K. Chem. *Soc. Rev.* **2016**, 45, 5107.

(2) (a) Wang, J.-L.; Wang, C.; Lin, W. *ACS Catal.* **2012**, *2*, 2630. (b) Wang, S.; Wang, X. *Small* **2015**, *11*, 3097. (c) Fateeva, A.; Chater, P. A.; Ireland, C. P.; Tahir, A. A.; Khimyak, Y. Z.; Wiper, P. V.; Darwent, J. R.; Rosseinsky, M. J. *Angew. Chem. Int. Ed*. **2012**, *51*, 7440.

(3) (a) Evans, J. D.; Sumby, C. J.; Doonan, C. J. *Chem. Soc. Rev*. **2014**, *43*, 5933. (b) Rojas, S.; Carmona, F. J.; Maldonado, C. R.; Horcajada, P.; Hidalgo, T.; Serre, C.; Navarro, J. A. R.; Barea, E. *Inorg. Chem.* **2016**, *55*, 2650.

(4) Chambers, M. B.; Wang, X.; Elgrishi, N.; Hendon, C. H.; Walsh, A.; Bonnefoy, J.; Canivet, J.; Quadrelli, E. A.; Farrusseng, D.; Mellot-Draznieks, C.; Fontecave, M. *ChemSusChem*. **2015**, *8*, 603.

(5) (a) Miras, H. N.; Yan, J.; Long, D.-L.; Cronin, L. *Chem. Soc. Rev.* **2012**, *41*, 7403. (b) Proust, A.; Matt, B.; Villanneau, R.; Guillemot, G.; Gouzerh, P.; Izzet, G. *Chem. Soc. Rev*. **2012**, *41*, 7605. (c) Ly, H. G. T.; Absillis, G.; Janssens, R.; Proost, P.; Parac-Vogt, T. N. *Angew. Chem. Int. Ed.* **2015**, *54*, 7391.

(6) (a) Wang, S.-S.; Yang, G.-Y. *Chem. Rev.* **2015**, *115*, 4893. (b) Lechner, M.; Güttel, R.; Streb, C. *Dalton Trans*. **2016**, *45*, 16716. (c) Sartorel, A.; Bonchio, M.; Campagna, S.; Scandola, F. *Chem. Soc. Rev*. **2013**, *42*, 2262.

(7) Walsh, J. J.; Bond, A. M.; Forster, R. J.; Keyes, T. E. *Coord. Chem. Rev*. **2016**, *306*, 217

(8) Juan-Alcañiz, J.; Gascon, J.; Kapteijn, F. *J. Mat. Chem*. **2012**, *22*, 10102.

(9) See for example (a) Maksimchuk, N. V.; Timofeeva, M. N.; Melgunov, M. S.; Shmakov, A. N.; Chesalov, Y. A.; Dybtsev, D. N.; Fedin, V. P.; Kholdeeva, O. A. *J. Catal. A*, **2008**, *257*, 315. (b) Granadeiro, C. M.; Barbosa, A. D. S.; Silva, P.; Almeida Paz, F. A.; Saini, V. K.; Pires, J.; de Castro, B.; Balula, S. S.; Cunha-Silva, L. *Appl. Catal. A: Gen.* **2013**, *453*, 316. (c) Han, J.; Wang, D.; Du, Y.; Xi, S.; Chen, Z.; Yin, S.; Zhou, T.; Xu, R. *Appl. Catal. A: Gen.* **2016**, *521*, 83.

(10) (a) Sun, C.-Y.; Liu, S.-X.; Liang, D.-D.; Shao, K.-Z.; Ren, Y.-H; Su, Z.-M. *J. Am. Chem. Soc*. **2009**, *131*, 1883. (b) Song, J.; Luo, Z.; Britt, D. K.; Furukawa, H.; Yaghi, O. M.; Hardcastle, K. I.; Hill, C. L. *J. Am. Chem. Soc*. **2011**, *133*, 16839. (c) Bajpe, S. R.; Kirschhock, C. E. A.; Aerts, A.; Breynaert, E.; Absillis, G.; Parac-Vogt, T. N.; Giebeler, L.; Martens, J. A. *Chem. Eur. J*. **2010**, *16*, 3926.

(11) Lan, Q.; Zhang, Z.-M.; Qin, C.; Wang, X.-L.; Li, Y.-G.; Tan, H.-Q. Wang, E.-B. *Chem. Eur. J.* **2016**, *22*, 15513.

(12) (a) Salomon, W. ; Roch-Marchal, C.; Mialane, P.; Rouschmeyer, P.; Serre, C.; Haouas, M.; Taulelle, F.; Yang, S.; Ruhlmann, L.; Dolbecq, A. *Chem. Commun*. **2015**, *51*, 2972. (b) Zhang, Z.-M.; Zhang, T.; Wang, C.; Lin, Z.; Long, L.-S.; Lin, W. *J. Am. Chem. Soc*. **2015**, *137*, 3197. (c) Kong, X.-J.; Lin, Z.; Zhang, Z.-M.; Zhang, T.; Lin, W. *Angew. Chem. Int. Ed.* **2016**, *55*, 6411. (d) Buru, C. T.; Li, P.; Mehdi, B. L.; Dohnalkova, A.; Platero-Prats, A. E.; Browning, N. D.; Chapman, K. W.; Hupp, J. T.; Farha, O. K. *Chem. Mat*. **2017**, *29*, 5174.

(13) Schaming, D.; Costa-Coquelard, C.; Sorgues, S.; Ruhlmann, L.; Lampre, I. *Appl. Catal. A: Gen.* **2010**, *373*, 160.

(14) Panagiotopoulos, A. ; Douvas, A. M.; Argitis, P.; Coutsolelos, A. G. *ChemSusChem* **2016**, *9*, 3213.

(15) Natali, M.; Deponti, E.; Vilona, D.; Sartorel, A.; Bonchio, M. ; Scandola, F. *Eur. J. Inorg. Chem*. **2015**, 3467.

(16) Morris, W.; Volosskiy, B.; Demir, S.; Gándara, F.; McGrier, P. L.; Furukawa, H.; Cascio, D.; Stoddart, J. F.; Yaghi, O. M. *Inorg. Chem.* **2012**, *51*, 6443.

(17) Feng, D.; Gu, Z.-Y.; Li, J.-R.; Jiang, H.-L.; Wei, Z.; Zhou, H.-C. *Angew. Chem. Int. Ed*. **2012**, *51*, 10307.
(18) Chen, Y.; Hoang, T.; Ma, S. *Inorg. Chem*. **2012**, *51*, 12600.
(19) Sasan, K.; Lin, Q.; Mao, C.; Feng, P. *Chem. Commun*. **2014**, *50*, 10390.
(20) (a) Vickers, J. W.; Lv, H.; Sumlinr, J. M.; Zhu, G.; Luo, Z.; Musaev, D. G.; Geletii, Y. V. ; Hill, C. L. *J. Am. Chem. Soc*. **2013**, *135*, 14110. (b) Huang, Z.; Luo, Z.; Geletii, Y. V.; Vickers, J. W.; Yin, Q.; Wu, D.; Hou, Y.; Ding, Y.; Song, J.; Musaev, D. G.; Hill, C. L.; Lian, T. *J. Am. Chem. Soc*. **2011**, *133*, 2068.
(21) Li, H.; Cao, X.; Zhang, C.; Yu, Q.; Zhao, Z.; Niu, X.; Sun, X.; Liu, Y.; Ma, L.; Li, Z. *RSC Adv*. **2017**, *7*, 16273.
(22) Mondloch, J. E.; Bury, W.; Fairen-Jimenez, D.; Kwon, S.; DeMarco, E. J.; Weston, M. H.; Sarjeant, A. A.; Nguyen, S. T.; Stair, P. C.; Snurr, R. Q.; Farha, O. K.; Hupp, J. T. *J. Am. Chem. Soc*. **2013**, *135*, 10294.
(23) Planas, N.; Mondloch, J. E.; Tussupbayev, S. J.; Borycz, J.; Gagliardi, L.; Hupp, J. T.; Farha, O. K.; Cramer, C. J. *J. Phys. Chem. Lett.* **2014**, *5*, 3716.
(24) Soriano-Lopez, J.; Musaev, D. G.; Hill, C. L., Galan-Mascaros, J. R.; Carbo, J. J.; Poblet, J. M. *J. Catal.* **2017**, *350*, 56.
(25) These concentrations correspond to the same molar amount of POM and MOF as 0.5 mg of $P_2W_{18}Co_4$@MOF-545.
(26) Xu, H.-Q.; Hu, J.; Wang, D.; Li, Z. ; Zhang, Q. ; Luo, Y. ; Yu, S.-H. ; Jiang, H.-L. *J. Am. Chem. Soc*. **2015**, *137*, 13440.
(27) Shiwon, R.; Klingan, K.; Dau, H.; Limberg, C. *Chem. Commun*. **2014**, *50*, 100.
(28) (a) Finke, R. G.; Droege, M. W.; Domaille, P. Inorg. Chem. 1987, 26, 3886; (b) Weakley, T. J. R.; Evans Jr., H. T.; Showell, J. S.; Tourné G. F.; Tourné, C. M. *J. Chem. Soc.,Chem. Commun*. **1973**, 139.
(29) Feng, D.; Gu, Z.-Y.; Li, J.-R.; Jiang, H.-L.; Wei, Z.; Zhou, H.-C. *Angew. Chem. Int. Ed*. **2012**, *51*, 10307
(30) Kelty, M. L. ; Morris, W. ; Gallagher, A. T. ; Anderson, J. S. ; Brown, K. A. ; Mirkin, C. A. ; Harris, T. D. *Chem. Commun*. **2016**, *52*, 7854.
(31) (a) Zhang, Z.-M.; Zhang, T.; Wang, C.; Lin, Z.; Long, L.-S.; Lin, W. *J. Am. Chem. Soc.* **2015**, *137*, 3197. (b) Kong, X.-J.; Lin, Z.; Zhang, Z.-M.; Zhang, T.; Lin, W. *Angew. Chem. Int. Ed.* **2016**, *55*, 6411.
(32) Aziz, A.; Ruiz-Salvador, A. R.; Hernandez, C. C.; Calero, S.; Hamad, S.; Grau-Crespo, R. *J. Mater. Chem. A* **2017**, *5*, 11894.

SYNOPSIS TOC